Terahertz transmission through ensembles of subwavelength-size metallic particles

K. J. Chau and A. Y. Elezzabi
Ultrafast Photonics and Nano-Optics Laboratory, Department of Electrical and Computer Engineering, University of Alberta, Edmonton T6G 2V4, Canada
(Received 11 April 2005; published 2 August 2005)

We demonstrate that terahertz radiation can coherently propagate through dense ensembles of subwavelength-size metallic particles over distances that are orders of magnitude greater than the skin depth. Collectively, the metal particle ensembles behave similar to a dispersive lossy dielectric. To fully explore this phenomenon, we investigate the effects of particle size, shape, metal type, and conductivity on the temporal characteristics of the transmitted radiation. In addition, we show that the transmission preserves the incident polarization state. Such an observation indicates that electromagnetic energy propagation across the extent of the particle ensemble is of a coherent nature. Finite difference time domain simulations of electromagnetic wave propagation in random metallic media support the experimental observations and show that electromagnetic energy transport is due to near-field plasmonic coupling between particles.

DOI: 10.1103/PhysRevB.72.075110 PACS number(s): 42.25.Dd, 71.45.Gm, 41.20.Jb, 42.25.Bs

Tailoring the electromagnetic response of materials via structural manipulation on sub-wavelength size scales has opened up new avenues in nanophotonics. In particular, recent interest has focussed on the exploration of extraordinary electromagnetic effects in subwavelength-size metallic media.[1–5] For instance, Wu *et al.*[1] have shown that the collective electromagnetic response of a subwavelength two-dimensional lattice of metallic wires can exhibit a reduced plasma frequency, thus behaving similar to a high-pass filter in the terahertz (THz) frequency regime. Moreover, two groups[2,3] have recently demonstrated that artificial magnetic materials at THz frequencies can be fashioned from nonmagnetic metals by using subwavelength split-ring resonators. In this configuration, the incident electric field drives current in the split rings, effectively producing a collection of subwavelength-size magnetic dipoles. Perhaps the most intriguing experiment is the recent discovery by Shelby *et al.*[4] demonstrating that a periodic collection of subwavelength metallic scattering elements can exhibit negative refractive index at microwave frequencies. It is noteworthy that previous investigations have examined the electromagnetic responses of *ordered* or artificially engineered metallic structures at either THz or gigahertz frequencies, since such long wavelengths allow for relatively simple fabrication of diverse, subwavelength-size structures. Strong near-field effects in these metallic structures have resulted in macroscopic electromagnetic responses that are uncharacteristic of its bulk counterpart. Accordingly, such unique photonic materials are attractive both for the development of next-generation photonic devices and for the fundamental understanding of light matter interaction on mesoscopic size scales.

The electromagnetic response of bulk metals is well described through the collective response of a sea of conduction electrons in the presence of an electromagnetic field. Such a description relies on the Drude permittivity $\varepsilon(\omega)$ which characterizes the electromagnetic response of metals at a frequency ω by $\varepsilon(\omega)=1-\omega_p^2/(i\Gamma\omega-\omega^2)$ where $\omega_p=ne^2/\varepsilon_0 m_e$ is the plasma frequency and Γ, n, m_e, e, and ε_0 are the damping frequency, electron density, electron mass, electron charge, and the free-space permittivity, respectively. For most metals, the plasma frequency is within the frequency range from the visible to the ultraviolet. For $\omega<\omega_p$, the real part of the permittivity is negative. In this frequency regime, electromagnetic waves incident on the metal are strongly reflected at the surface and, inside the metal, exist as evanescent waves within a skin depth that is typically in the nanometer range. Despite the success of the Drude model in describing these general properties of metals at low frequencies of the infrared, it implicitly assumes that a metallic medium is of a continuous nature, neglecting the effect of the metal's structure. In particular, when the dimensions of the metallic structure are of subwavelength size, the electromagnetic properties of the medium can be strongly influenced by its microscopic geometrical features. In this regime, near-field interaction, which is highly sensitive to the structure, spatial order, and geometry of the metallic medium, can dominate, and the Drude model becomes limited in describing the global optical properties of the entire medium.

In this work, a follow up of our initial report in Ref. 5, we present findings showing that *random* metallic media can also show extraordinary optical properties. In particular, we find that THz radiation can transmit through ensembles of subwavelength-size metallic particles over distances five orders of magnitude greater than the radiation bulk absorption depth. Effectively, the particles exhibit electromagnetic properties akin to a dispersive lossy dielectric. That is, despite the local negative real permittivity of the individual metallic particles, the collective ensemble of particles demonstrates an effective positive real permittivity. In addition to this extraordinary transmission phenomenon, we find that the transmitted radiation preserves the incident polarization state. This observation strongly indicates that, despite the random nature of the ensemble, electromagnetic energy propagation across the extent of the medium is coherent. Such findings further elucidate the origin of the enhanced transmission phenomenon and open the door to the application of random metallic materials for photonic and spectroscopic applications.

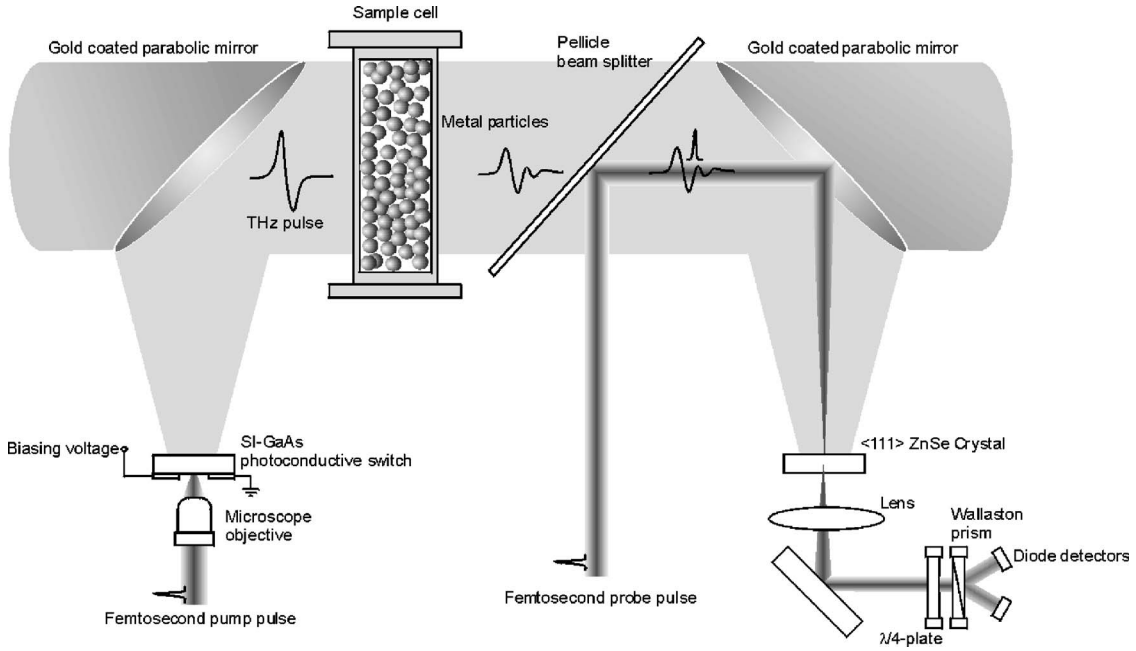

FIG. 1. Schematic of the free-space THz generation and electro-optic detection setup used to characterize the THz electric field transmission through the metallic particle ensembles.

To fully explore the extraordinary transmission through subwavelength metallic particles in the THz regime, we have systematically investigated the dependence of the transmission on a wide range of variables such as particle dimension, shape, and conductivity. Frequency selective electromagnetic coupling is precluded by employing densely packed, near-touching metallic particles that are randomly oriented and possess no particular spatial order or symmetry in three-dimensional space. Accordingly, a broadband THz source is necessary to probe the full electromagnetic response of the random metallic particle ensembles over a wide frequency range. Moreover, in order to study the dynamic behavior of the enhanced transmission, we require access to both the temporal characteristics of the transmitted electric field and its phase coherence. To obtain such time-resolved and phase-sensitive measurements, we employ broadband THz time domain spectroscopy. As shown in Fig. 1, free-space THz pulses are generated via free-carrier photoexcitation of a 100-μm photoconductive gap on a semi-insulating GaAs substrate. The photoconductive gap is biased at 20 $V_{p\text{-}p}$ and a 120 mW pump pulse from a 20-fs Ti:sapphire oscillator is used to generate transient charge carriers within the photoconductive gap. The resulting linearly polarized, 1-ps wide, broadband far-infrared pulses are collected and collimated to a diameter of 2 cm by an f/1.0, gold coated parabolic mirror. The collimated THz pulses are subsequently directed upon a 6 cm diameter polystyrene sample cell with a variable thickness L which houses the metallic particles. The transmitted THz pulse is propagated collinearly with a temporally synchronized 10 mW probe pulse, and a second parabolic mirror focuses both the free-space THz pulse and the probe pulse onto an electro-optic crystal (ZnSe $\langle 111 \rangle$). An optical detection scheme incorporating a $\lambda/4$ plate, a Wallaston prism, and differential photodetectors extracts the polarization modulation induced by the THz electric field signal, while lock-in detection is carried out at the biasing voltage frequency (54 KHz) to further optimize the signal-to-noise ratio. Since the electro-optic response of the $\langle 111 \rangle$ ZnSe crystal is sensitive to the THz pulse polarization in addition to the synchronization between the THz and probe pulses, this coherent detection scheme accesses both the time-domain and polarization characteristics of the transmitted THz electric field.

Given the fact that the plasma frequencies of metals typically range from the visible to the ultraviolet, the real permittivity of bulk metals is negative at THz frequencies. Thus, it is anticipated that the metallic particles exhibit weak collective THz transmission since the particle dimensions and interparticle spacing are significantly smaller than the radiation wavelength, and bulk propagating electromagnetic modes are precluded. Remarkably, however, significant ($\leqslant 20\%$) THz transmission is measured through metallic particles which are collectively several orders of magnitude thicker than the radiation skin depth. The enhanced THz transmission is not specific to metal type and has been observed through a wide variety of metals and particle sizes. To highlight this universality, Fig. 2(a) depicts transmitted THz pulses through $L=1.2$ mm thick samples of densely packed Cu, Cr, and Al particles having dimensions of 71 ± 20, 150 ± 50, and 400 ± 100 μm, respectively. Globally, the optical properties of the subwavelength-size metallic particle ensembles can be described by an effective permittivity. While the real part of the permittivity of nearly all metals is negative at THz frequencies, which renders them opaque to THz radiation, the significant transmission measured through the collection of metallic particles indicates that their effective permittivity attains a positive value. Thus, electromagnetic modes are permitted to propagate through the metallic particle ensembles. The time-resolved signals depicted in Fig. 2(a) are characterized by temporally delayed and broadened

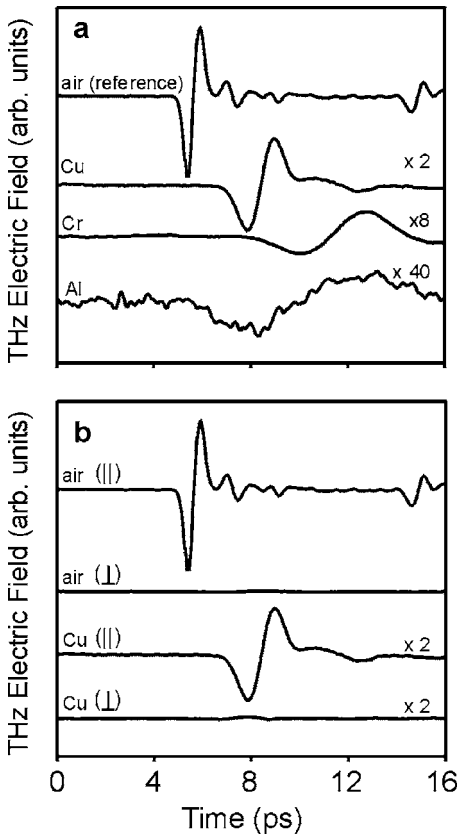

FIG. 2. (a) Experimental transmitted THz electric fields measured through an empty cell and through 1.2-mm-thick samples of irregularly shaped Cu, Cr, and Al particles having mean dimensions of 71 ± 20, 150 ± 50, and 400 ± 100 μm, respectively. The transmitted fields are polarized parallel to the incident THz polarization. (b) Negligible transmission is measured in the perpendicular polarization, as shown for the free-space THz pulse and the transmitted THz pulse through the Cu particle ensemble.

field oscillations relative to the reference pulse transmitted through an empty cell. When compared to an air path, the relative delays introduced by the $L=1.2$ mm Cu, Cr, and Al particle ensembles are 2.6 ± 0.1, 4.8 ± 0.1, and 3.0 ± 0.1 ps, respectively. The transmitted electric fields have drastically disparate amplitudes. Compared to the reference THz pulse, the field amplitude through the Cu ensemble is 20.7%, while the relative electric fields transmitted through the Cr and Al ensembles are only 3.4 and 1.0%, respectively. The large variation in the amplitude and the arrival time of the transmitted THz pulses through the different metallic media reveals a rich dependence of the transmission phenomenon on particle shape, size, and metal type. These variables will be explored further in this work.

To characterize the transmitted THz electric field polarization state, we vary the orientation φ of the $\langle 111\rangle$ ZnSe crystal with respect to the probe pulse polarization. In this manner, the transmitted THz electric field components parallel and perpendicular to the incident THz pulse can be measured independently.[6] Interestingly, despite the inherent opacity of the metallic particles and the random nature of the particle collection, polarization characterization shows that all of the transmitted electric fields preserve the incident polarization. As representatively shown for Cu in Fig. 2(b), high polarization purity is evident from the insignificant relative amplitude of the THz electric field component measured in the perpendicular direction ($<4\%$, corresponding to a polarization purity of $>96\%$). This is congruent with measurements of the parallel and perpendicular components of the polarized THz pulse propagating through air (99.3% polarization purity). The high polarization purity of the transmitted electric fields though the metallic particle ensembles suggest that electromagnetic energy propagates coherently through the metallic medium, shedding insight into the origin of the enhanced transmission.

As mentioned in our previous work,[5] the underlying, physical origin of the enhanced transmission is attributed to plasmonic electromagnetic energy propagation across the ensembles of subwavelength-size particles. The incident far-infrared pulse excites plasmon oscillations of the conduction electrons at the surface of individual metallic particles, effectively producing a collection of oscillating dipoles $p(t)$. The electric field $E(r,t)$ associated with the plasmon dipole, consists of quasistatic ($\propto 1/r^3$), near-field ($\propto 1/r^2$), and far-field ($\propto 1/r$) terms and is expressed as[7]

$$E(r,t)=\frac{1}{4\pi\varepsilon_0}\left(\frac{1}{r^3}p(t)+\frac{1}{r^2c}\frac{\partial p(t)}{\partial t}+\frac{1}{c^2r}\frac{\partial^2 p(t)}{\partial t^2}\right), \quad (1)$$

where r is the distance from the dipole and c is the speed of light. For closely spaced particles, high electric fields near the particle surface dominate and lead to strong near-field electromagnetic coupling between particles. Sequential electromagnetic coupling between closely spaced particles transports electromagnetic energy across the particle ensemble, and at the edge of the sample, the surface plasmon currents radiate into the far field. The far-field transmission amplitude is determined by the resistive losses experienced by the propagating plasmon as well as intraparticle plasmon scattering, while the polarization of the transmitted electric field is correlated with the coherence of the electromagnetic energy transport mechanism. Such coherence is determined by the effect of polarization-randomizing scattering events in relation to the plasmon coherence length. The previous observations of polarization preservation of the transmitted THz electric field suggest weak plasmon scattering occurring within distances less than the plasmon coherence length.

To explicitly illustrate the origin of the enhanced transmission, THz light propagation in the collection of metallic particles is investigated by modeling the physical phenomena using numerical two-dimensional finite difference time domain (FDTD) solutions to Maxwell's equations. The FDTD technique provides a powerful method to describe light propagation in complex structures. Coupling of incident THz light into the plasmonic oscillations of the metal is accounted for by the Drude model of $\varepsilon(\omega)$. By recasting relation $\mathbf{D}=\varepsilon(\omega)\mathbf{E}$, where $\mathbf{D}$ and $\mathbf{E}$ are the displacement and electric fields, respectively, into the time domain through Fourier transformation, we generate the supplementary equation

$$\Gamma d\mathbf{D}/dt+d^2\mathbf{D}/dt^2=\omega_p^2\varepsilon_0\mathbf{E}+\Gamma\varepsilon_0 d\mathbf{E}/dt+\varepsilon_0 d^2\mathbf{E}/dt^2, \quad (2)$$

where ε_o is the permittivity of free-space. In combination with the equations $\partial\mathbf{D}/\partial t=\nabla\times\mathbf{H}$ and $\partial\mathbf{H}/\partial t=-(1/\mu_o)\nabla$

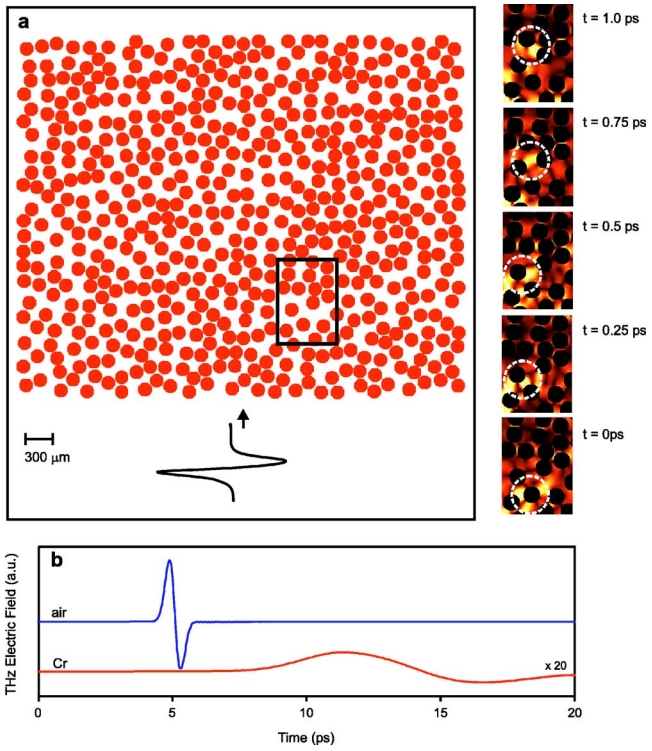

FIG. 3. (Color online) (left) Simulation structure used in the FDTD simulations consisting of an ensemble of 150-μm circular particles. The panels to the right depict magnified images of the boxed region and show the propagation sequence of the THz field magnitude over a 1-ps duration. The sequence of images illustrates that electromagnetic energy transport through the metallic particle ensemble is governed by nearest-neighbor coupling. (b) Simulated transmitted THz electric field through the L=4-mm sample of 150-μm Cr particles along with a reference pulse transmitted through an air path.

$\times \mathbf{E}$, where $\mathbf{H}$ is the magnetic field, the fields $\mathbf{E}$, $\mathbf{D}$, and $\mathbf{H}$ are solved for all time and space using a central differencing scheme.[8] In the two-dimensional simulations, the random medium is modeled as a collection of circular particles that extend infinitely in the third dimension. It should be noted that a three-dimensional model would enable a more complete picture of our experiments as the plasmon resonances associated with the particles depends on the dimensionality. In three dimensions, the plasmon fields are effectively confined to a smaller surface area, which would appear as an enhancement in the local fields. However, full three-dimensional FDTD calculations over the length scales of the transmission phenomenon require enormous computational effort in comparison to the current model and are not currently feasible. The two-dimensional simulations are adequate in illustrating the underlying physics of the phenomenon, and the conclusions of the simulations can be employed to interpret the experimental results. Figure 3 demonstrates single cycle, 1-ps wide THz pulse illumination of an L=4.0 mm sample of randomly placed Cr particles. The Cr permittivity is described through fitting and extrapolation of the Drude model to experimental data from Ref. 9. The circular particles have a mean diameter of 150 μm and a 0.5 packing fraction. The time evolution of the electric field magnitude from t=0 to 1.0 ps in a small region of the medium is shown in Fig. 3. At t=0 ps, surface plasmon oscillations are evident from the high electric fields near the particles' surfaces. At later times, $t>0$ ps, the images clearly illustrate the nature of plasmonic near-field coupling and subsequent propagation. Over the 1-ps interval, the high plasmonic surface fields propagate via nearest neighbor coupling from particle to particle across the metallic medium over a distance of $\sim$600 μm. Thus, through such near-field particle-to-particle coupling, the THz electromagnetic field is transported across subwavelength-size metallic particle ensembles over distances several orders of magnitude larger than the metal's skin depth [$\sim$40 nm at 1 THz for Cr (Ref. 5)]. The average transmission through the entire medium is measured by integrating the total electric field incident on a line detector placed at the back of the sample, emulating the experimental detection scheme. As shown in Fig. 3(b), the FDTD simulation accurately predicts the general characteristics of the transmission through the metallic particle ensemble. The simulated transmitted electric field through the L=4 mm sample of 150-μm Cr particles is delayed and broadened with respect to the THz pulse transmitted through an air path, and the significant ($\sim$1.4%) transmitted electric field amplitude accords with previous experimental observations.

It is well known that near-field plasmonic phenomenon is inherently dependent on the size of the metallic particles.[10–12] As the size of the particles approaches very small (nanometer) scales, it is expected that the ensemble approaches the limit of a dense, nontransmitting bulk metal. Similarly, in the opposing limit, the ensemble behaves as a nontransmitting bulk when the particle dimensions are much larger than the wavelength. To investigate the effect of particle size on the enhanced transmission, we have performed comparative transmission measurements using two Cr particle ensembles with mean dimensions of 150±50 and 40±20 μm and similar volume packing fractions of 0.5. By comparing the THz electric field transmission through the two samples shown in Fig. 4, it is evident that the transmitted electric field through the 150-μm Cr particles exhibits temporally broader oscillations and a lower bandwidth than the transmitted electric field through the 40-μm particles. For a representative sample length of 0.6 mm, the 40- and 150-μm particle ensembles show transmission bandwidths of 0.35 and 0.23 THz, respectively. As illustrated in Fig. 4(e), the higher frequencies (>0.4 THz) of the transmitted electric field are preferentially extinguished as the particles' size is reduced from 150 to 40 μm. Such a bandwidth reduction with increasing particle size occurs in conjunction with a central frequency shift from 0.20 to 0.24 THz as the particle size decreases from 150 to 40 μm. This spectral blueshift of the transmitted THz pulse is attributed to a blueshift of the individual particle plasmon as the particle size decreases. It is interesting to note that at optical frequencies similar blueshifting with decreasing particle size has been observed in the plasmon resonances associated with metallic nanoparticles.[10,13]

As evident from Figs. 4(c) and 4(d), the relative THz electric field arrival time is also dependent on the particle size. The relative delay of the transmission through the

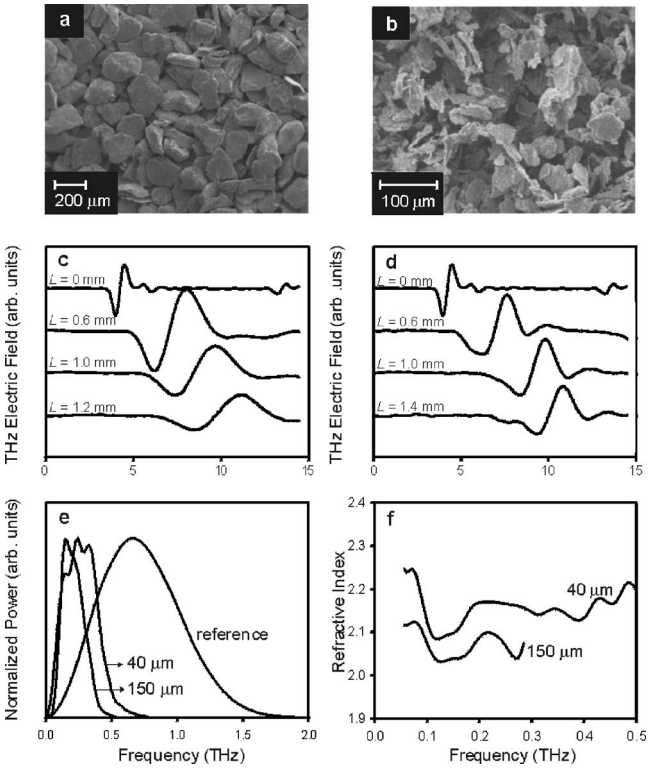

FIG. 4. Scanning electron microscope images of Cr particles having dimensions of (a) 150±50 and (b) 40±20 μm. (c) and (d) depict the experimental transmitted THz electric field through the 150- and 40-μm-size Cr particles, respectively, for various sample thicknesses, in addition to the reference THz pulse transmitted through an empty cell. (e) shows the power spectrum of the experimental transmission through the empty cell, a L=0.6-mm sample of the 150-μm Cr particles and a L=0.6-mm sample of the 40-μm Cr particles. Illustrated in (f) are the experimentally measured effective refractive indices across the transmission bandwidths for the two Cr particle ensembles.

40-μm Cr particles indicates slowed plasmonic propagation. By measuring the arrival times of the first peak of the transmitted THz pulses as a function of L, propagation velocities of $0.47c\pm0.01c$ and $0.50c\pm0.01c$ are measured through the 40- and 150-μm particle ensembles, respectively. Intuitively, this can be understood as arising from the increased metal surface area in the smaller Cr particles, which augments the electromagnetic energy propagation distance. This interpretation will be further supported by FDTD simulations in later discussions within this work. To analyze the dispersion characteristics of the two Cr ensembles, we determine their effective frequency-dependent refractive indices $n_{\text{eff}}(\omega)$. This is accomplished by measuring the transmitted electric fields for two sample thicknesses of L and $L+\Delta L$. From the spectral phase accumulation $\phi_{\Delta L}(\omega)=\phi_L(\omega)-\phi_{L+\Delta L}(\omega)$ of the transmitted electric field over the sample length change, the refractive index can be determined from the relation $n_{\text{eff}}(\omega)=k\Delta L/\varphi_{\Delta L}(\omega)$, where $k=2\pi/\lambda$ is the wave vector. Shown in Fig. 4(f) are the refractive indices of the 40- and 150-μm particle ensembles obtained by averaging six independent measurements for each particle collection. It is evident that reducing the granular dimensions increases the effective refractive index of the metallic particle ensembles. The refractive indices for the 40- and 150-μm Cr samples are approximately 2.0 and 2.1, respectively, over their transmission bandwidths. Interestingly, the refractive indices of these Cr samples are characterized by large dispersion across the bandwidth of the transmitted electric field, which causes pulse width broadening for increasing sample length.[5] Again, we can draw upon the analogy of the dense ensemble of metallic particles collectively behaving as a dispersive, lossy dielectric having positive real permittivity in the THz regime.

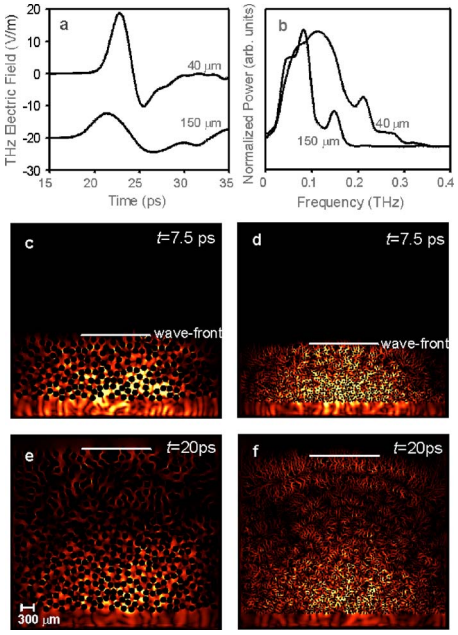

FIG. 5. (Color online) (a) FDTD simulations of the temporal THz transmitted electric fields through L=4-mm ensembles of Cr particles with mean dimensions of 40 and 150 μm. Note that the transmitted pulse through the smaller Cr particles arrives at a later time. (b) The power spectra of the simulated transmission through the two particle ensembles. (c) and (d) illustrate the THz field magnitude in the 150- and 40-μm Cr particle ensembles, respectively, at t=7.5 ps. THz field magnitudes at t=20.0 ps in the 150- and 40-μm Cr particle ensembles are shown in (e) and (f), respectively.

To further investigate the effect of particle size, the experimental results are compared with FDTD simulations. The simulated THz transmission through 4-mm-thick ensembles of Cr particles with mean dimensions of 40 and 150 μm are shown in Fig. 5. The simulated transmitted electric field through the smaller particles is temporally delayed [Figure 5(a)] and spectrally wider [Figure 5(b)] with respect to the transmitted electric field through the larger particles. Such behavior is in accordance with previous experimental observations. To visualize the origin of this delay, snapshots of the electromagnetic wave progression through the two Cr particle ensembles are shown in Figs. 5(c)–5(f). At t=7.5 ps, the free-space THz pulse incident on the ensemble couples into surface plasmon oscillations of the metallic particles. From t=7.5 to 20 ps, electromagnetic energy propagates as a high intensity wave-front explicitly highlighted in Figures 5(c)–5(f). This wavefront, which corresponds to the mea-

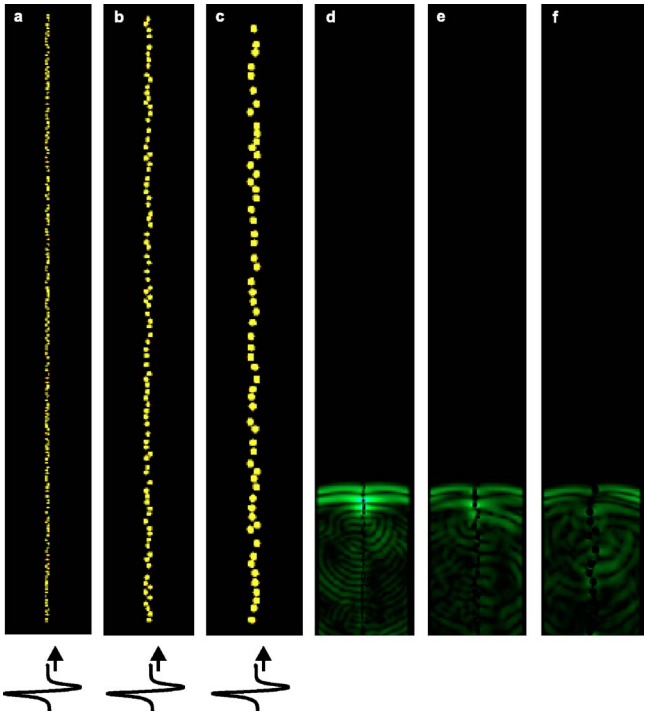

FIG. 6. (Color online) (a), (b), and (c) depict the 50, 100, and 150 μm Cr particle chains used in the FDTD simulations, respectively. The chain lengths are 12 mm. (d), (e), and (f) depict the THz field magnitudes in the 50-, 100-, and 150-μm Cr particle chains, respectively, at an identical time after excitation with a 1-ps wide THz pulse. Note that the all the THz wavefronts progress at the same velocity for the three particle chains.

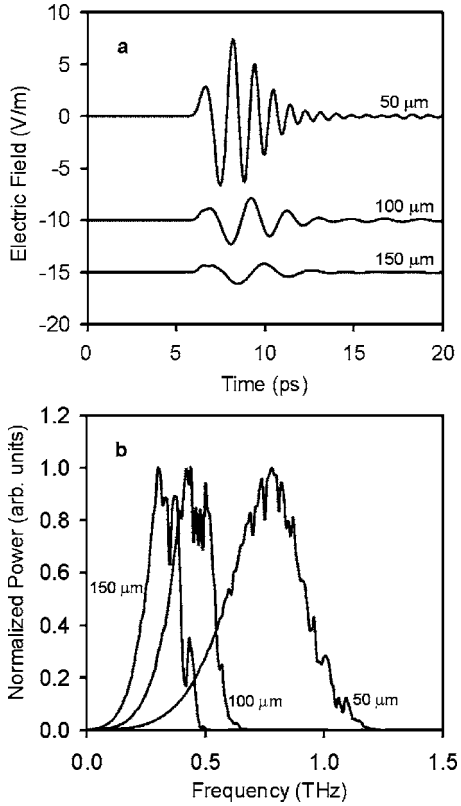

FIG. 7. FDTD simulations of (a) the temporal THz transmitted electric field and (b) the spectral power transmission through the 12-mm-long Cr chains consisting of 50, 100, and 150 μm size particles.

sured far-field transmitted electric field, propagates through the metallic medium via nearest-neighbor coupling. Examination of the images at $t=20$ ps [Figs. 5(e) and 5(f)] clearly show that the wavefront progresses slower through the 40-μm Cr particles relative to the 150-μm particles. By tracking the wavefront progression through the metallic media, plasmon propagation velocities of $0.62c\pm0.01c$ and $0.66c\pm0.01c$ are measured through the 40- and 150-μm particle ensembles, respectively. These values are comparable with the experimental measured values.

The FDTD simulations enable a comprehensive interpretation of slower wave propagation in ensembles of smaller particles. Due to the random nature of the medium, there is inherent directionality scramble of the electromagnetic wave with each nearest-neighbor interaction. By increasing the number of particles across a given sample length (by decreasing the particle size), increased directionality scramble augments the effective energy propagation distance, causing a delay of the transmitted radiation. To demonstrate that the origin of this delay is due to directionality scramble, we perform FDTD simulations where directionality scramble is absent. In these simulations, the THz pulse is confined to propagate along 12-mm long chains of randomly positioned particles with sizes of 50, 100, and 150 μm, as shown in Figs. 6(a)–6(c). In such configurations, lateral confinement results in unidirectional near-field plasmonic coupling. As shown in Figs. 6(d)–6(f), snapshots of the electric field magnitudes at a particular time show that the THz pulses propagate at similar velocities through the different particle chains. Accordingly, the transmitted THz pulses measured at the end of the laterally confined particle chains arrive at matched times as evident in Fig. 7(a). The transmitted field associated with the chain of 50-μm-size particles consists of higher frequency oscillations than that associated with the 100- and 150-μm particle chains. As shown in Fig. 7, the 50-, 100-, and 150-μm particle chains exhibit bandwidths of 0.36, 0.25, and 0.15 THz, respectively. The increasing bandwidth with decreasing particle size is accompanied by a shift of the central frequency toward higher frequencies, consistent with the previous experimental trend shown in Fig. 4(e).

Due to inherent surface sensitivity of plasmonic phenomena, particle shape is a key parameter in the interaction of light with subwavelength metallic particles.[10,14,15] To qualitatively investigate the effect of particle shape on the plasmonic transmission, we employ two separate Cu samples consisting of spherical and irregularly shaped particles. Figure 8 depicts scanning electron microscope images of the spherical and irregularly shaped samples having mean particle dimensions of 83 ± 15 and 71 ± 20 μm, respectively. Since the size difference between the particles is 2.4% of the central THz pulse wavelength of 500 μm, to a good approximation, the effect of particle size in the comparative measurements is insignificant. As illustrated in time-domain THz signals in Fig. 8(c), particle shape does not strongly influence the transmitted temporal pulse shape. Similarly, the transmission bandwidth does not vary between the irregular and

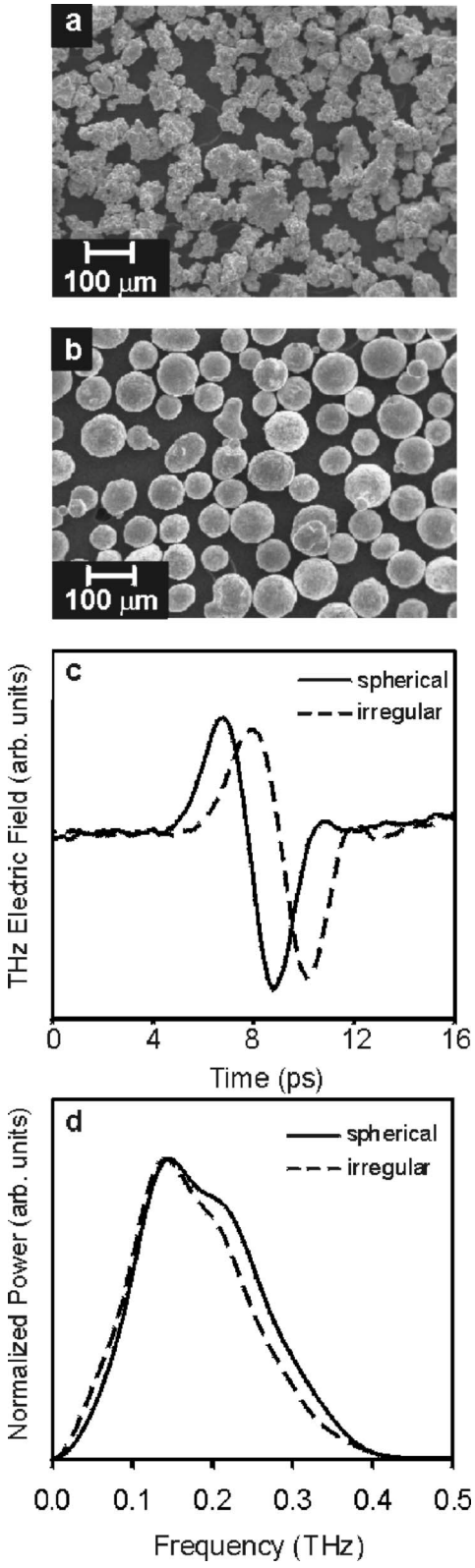

FIG. 8. Scanning electron microscope images of (a) irregular and (b) spherical Cu particles of mean dimensions 71 ± 20 and 83 ± 15 μm, respectively. (c) depicts the experimental temporal THz transmitted electric field through $L=2.1$-mm samples of the irregular and spherical Cu particles, and (d) shows their corresponding power spectra.

spherical Cu particles [Fig. 8(d)], indicating that the plasmon resonances associated with the individual Cu particles do not strongly depend on the exact particle shape. However, the THz pulse transmitted through the spherical Cu particles arrives earlier than the transmitted electric field through the irregular particles. For the representative sample length of 2.1 mm, the transmitted electric field through the spherical Cu particles arrives 1.2 ± 0.1 ps earlier than that through the irregularly shaped Cu particles. Such a delay suggests that particle irregularity causes slowed plasmonic propagation through the metallic particles. The origin of the significant delay is understood as follows: since the transmission is mediated by plasmonic fields confined to the particles' surfaces, increasing the particle surface area effectively increases the plasmonic propagation distance, which manifests as a delay in the transmitted electric fields. As evident in Fig. 8, particle irregularity also slightly diminishes the plasmonic transmission through the metallic media. For a sample length of 2.1 mm, the transmitted field through the irregularly shaped Cu particles is 8% smaller than the transmission through the spherical Cu particles. The decreased transmission is attributed to scattering losses at the surface of the irregularly shaped particles, which reduces the transmitted electric field amplitude.

In addition to particle size and shape, the photonic transport properties of the metallic ensembles are dependent on the electronic characteristics of the metal. In high conductivity metals, electrons exhibit a long mean free path, which minimizes resistive loss associated with electron scattering. To study the effect of metal conductivity on the enhanced transmission, we have performed comparative measurements of the transmission through Cu and $Cu_{95}Sn_5$ alloy particles. These samples have been selected due to their identical physical properties, since both samples consist of 83 ± 15 μm diameter spheres, as illustrated in Fig. 9. However, due to the lower conductivity of the $Cu_{95}Sn_5$ alloy particles as compared to pure Cu, we anticipate that plasmonic transmission through Cu will exhibit less attenuation. Indeed, as shown in Fig. 9, the transmission through the $L=2.1$ mm Cu sample is dissimilar from the transmission through the $L=2.1$ mm $Cu_{95}Sn_5$ sample. The peak-to-peak amplitude of the Cu transmission is 1.3 times larger than the transmission through $Cu_{95}Sn_5$, directly indicating decreased plasmonic attenuation. Moreover, the transmitted electric field through the Cu particles arrives slightly earlier (0.2 ± 0.1 ps) than that through the $Cu_{95}Sn_5$ particles. Despite discrepancies in the amplitudes and arrival times of the transmitted pulses, the pulse shape and frequency spectra of the transmission through the granular Cu and $Cu_{95}Sn_5$ do not differ within experimental error, as evident in Fig. 9. The congruent transmission spectra are attributed to the similar microscopic structural features and particle sizes of the two metallic samples. To further illustrate this effect, we perform FDTD simulations of THz transmission through two identical particle ensembles composed of dissimilar metals having significantly different conductivities in the far-infrared regime. Here, we have employed W and Cu metals since the Drude parameters for the permittivity of both metals are known.[16] Figure 9 shows the simulated time domain transmission through 2-mm-thick samples of W and Cu particles having diameters of 80 μm.

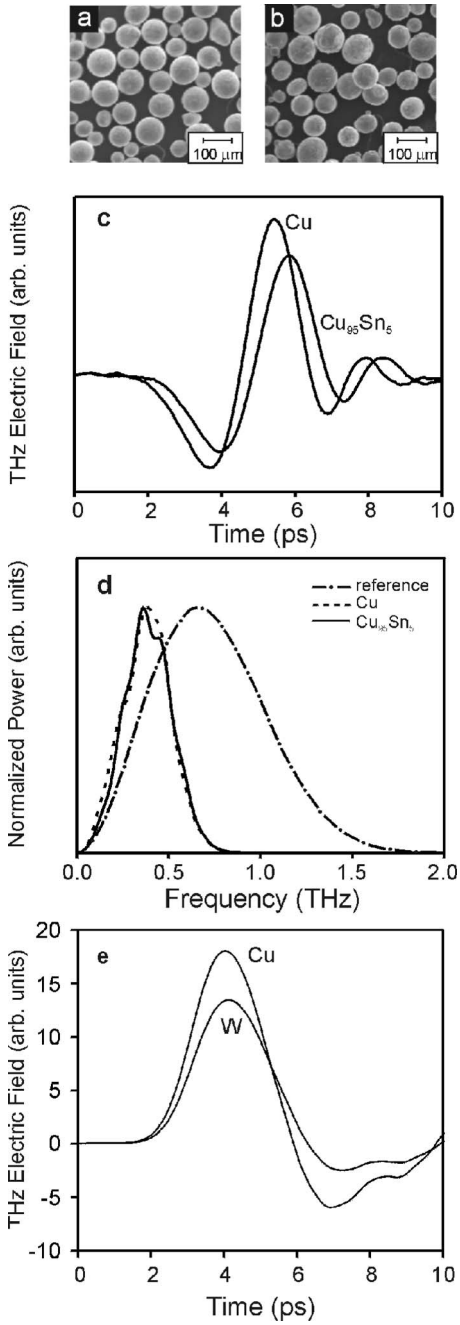

FIG. 9. Scanning electron microscope images of (a) $Cu_{95}Sn_5$ and (b) Cu particles, both having mean dimensions 83 ± 15 μm. (c) depicts the experimental temporal THz transmitted electric field through $L=2.1$-mm samples of $Cu_{95}Sn_5$ and Cu particles, and (d) illustrates their corresponding power spectra. Shown in (e) are FDTD simulations of the THz transmitted electric fields through identical $L=2$-mm-thick samples of 80-μm-diameter W and Cu particles.

In accordance with experimental observations, the transmission pulse shape does not change by altering the conductivity. However, the simulated transmission amplitude through Cu is slightly larger relative to the transmission through W due to decreased resistive loss. FDTD simulations qualitatively confirm that the metal conductivity directly affects the plasmonic loss, which is evident in the transmission amplitude.

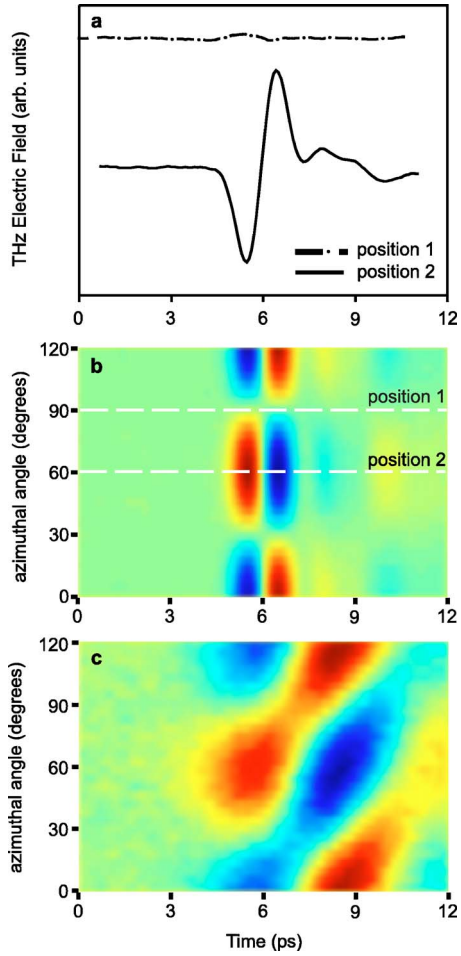

FIG. 10. (Color online) (a) Measured THz transmitted pulses for $L=0.6$-mm sample of 71 ± 20-μm nonspherical Cu particles in the perpendicular and parallel polarizations. These measurements correspond to the electric field component at 180° and 270° shown in (b). The normalized THz electric field amplitudes versus the azimuthal angle and time for (b) $L=0.6$ mm and (c) $L=7.0$ mm samples of Cu particles. Note that the zero times in (b) and (c) are not referenced to each other.

Despite the coherent nature of near-field electromagnetic coupling, initially, it seems perplexing that a random metallic medium extending over several orders of magnitude longer than the skin depth would preserve the incident polarization in transmission. To understand this effect, we investigate the influence of sample length on the transmitted THz electric field polarization. The polarization is characterized by varying the orientation of the $\langle 111 \rangle$ ZnSe crystal with respect to the probe pulse polarization. For the experimental geometry, the electro-optic response of the $\langle 111 \rangle$ ZnSe crystal at $\varphi=0°$, 60°, and 120° correspond to the transmitted THz component polarized parallel to the incident THz pulse, while the responses at $\varphi=30°$ and 90° correspond to electric field components along the perpendicular direction.[6] By sampling the transmitted THz fields from $\varphi=0°$ to $\varphi=120°$, the entire THz electric field distributed about the azimuthal angle is measured. Figures 10(b) and 10(c) map the experimentally mea-

sured temporal behavior of the transmitted electric field as a function of the azimuthal angle for $L=0.6$- and 7.7-mm-thick ensembles of 71 ± 20-μm Cu particle. For the $L=0.6$-mm-thick sample, the transmission preserves the incident linear polarization as evidenced by the threefold symmetry of the transmitted THz electric field, where maxima occur at 0°, 180°, and 360° and zero electric field is measured at 90° and 180°. The high polarization purity suggests the insignificant influence of polarization-randomizing scattering events in the relatively thin sample relative to the plasmon coherence length. However, the temporal electric field map versus φ shows entirely different behavior using the $L=7.7$-mm-thick sample. The transmitted field is temporally broader, as anticipated for increasing sample thickness.[5] More importantly, electric field components present at 90° and 180° indicate that the polarization purity is significantly compromised in the thicker sample. The reduced polarization purity is attributed to an increased probability of polarization randomizing scattering events in the thicker medium, which impairs the overall coherence of electromagnetic energy transport.

The experimental results confirm that dense ensembles of subwavelength-size metallic particles can exhibit extraordinary transparency at THz frequencies. The effects of particle size, particle shape, metal type, and conductivity on the temporal characteristics of the transmitted electric field have been experimentally explored. In addition, we show that the transmitted radiation preserves the incident polarization state, indicating that the transmission phenomenon is coherent. Numerical simulations using the FDTD technique further interpret the observed phenomenon and elucidate the electromagnetic transport mechanisms. In particular, the extraordinary transmission is attributed to near-field electromagnetic coupling between closely spaced particles across the extent of the medium. These unique findings open the door to the application of random metallic materials for future photonic applications such as dynamic filtering. Due to the inherent surface sensitivity of this phenomenon, we are currently exploring its potential application in time-domain THz spectroscopy analysis and detection of adsorbed monolayers.

This work was supported by the Natural Sciences and Engineering Research Council of Canada (NSERC), Canada Research Chairs Program (CRC), Canadian Foundation for Innovation (CFI), and the Alberta Ingenuity Fund. K.J.C. acknowledges the Alberta Ingenuity Fund, ICORE, and NSERC for financial support.

[1] D. Wu, N. Fang, C. Sun, X. Zhang, W. J. Padilla, D. N. Basov, D. R. Smith, and S. Shultz, Appl. Phys. Lett. **83**, 201 (2003).
[2] T. J. Yen, W. J. Padilla, N. Fang, D. C. Vier, D. R. Smith, J. B. Pendry, D. N. Basov, and X. Zhang, Science **303**, 1494 (2004).
[3] S. Linden, C. Enkrich, M. Wegener, J. Zhou, T. Koschny, and C. M. Soukoulis, Science **306**, 1351 (2004).
[4] R. A. Shelby, D. R. Smith, and S. Schultz, Science **292**, 77 (2001).
[5] K. J. Chau, G. D. Dice, and A. Y. Elezzabi, Phys. Rev. Lett. **94**, 173904 (2005).
[6] J. F. Holzman and A. Y. Elezzabi, Appl. Phys. Lett. **81**, 2294 (2002).
[7] D. H. Auston, K. P. Cheung, and P. R. Smith, Appl. Phys. Lett. **45**, 284 (1984).
[8] A. Taflove, *Computational Electrodynamics* (Artech House, Boston, 1995).
[9] *Handbook of Optical Materials*, edited by M. Weber (CRC Press, New York, 2003).
[10] K. L. Kelly, E. Coronado, L. L. Zhao, and G. C. Schatz, J. Phys. Chem. B **107**, 668 (2003).
[11] B. Lamprecht, G. Schider, R. T. Lechner, H. Ditlbacher, J. R. Krenn, A. Leitner, and F. R. Aussenegg, Phys. Rev. Lett. **84**, 4721 (2000).
[12] J. R. Krenn, A. Dereux, J. C. Weeber, E. Bourillot, Y. Lacroute, J. P. Goudonnet, G. Schider, W. Gotschy, A. Leitner, F. R. Aussenegg, and C. Girard, Phys. Rev. Lett. **82**, 2590 (1999).
[13] T. Klar, M. Perner, S. Grosse, G. von Plessen, W. Spirkl, and J. Feldmann, Phys. Rev. Lett. **80**, 4249 (1998).
[14] J. P. Kottman, O. J. F. Martin, D. R. Smith, and S. Shultz, Opt. Express **6**, 213 (2000).
[15] M. Futamata, Y. Maruyama, and M. Ishikawa, J. Phys. Chem. B **107**, 7607 (2003).
[16] M. A. Ordal, L. L. Long, R. J. Bell, S. E. Bell, R. R. Bell, R. W. Alexander, Jr., and C. A. Ward, Appl. Opt. **22**, 1099 (1983).